

CONFERENCES AND SYMPOSEA

PACS numbers: 68.65. – k, 73.20.Mf, **78.67. – n**

Nano-optical elements for surface plasmon waves (50th anniversary of the Institute of Spectroscopy, Russian Academy of Sciences)

P N Melentiev, V I Balykin

DOI: https://doi.org/10.3367/UFNe.2018.06.038415

Contents

Abstract. The main results obtained recently at the Laboratory of Laser Spectroscopy, Institute of Spectroscopy of the Russian Academy of Sciences in researching and developing various 2D optical elements for surface plasmon waves and their characterization using near- and far-field methods are presented. They include an optical medium for plasmon waves, a plasmon interferometer, a parabolic mirror for focusing plasmon waves, a dielectrically loaded plasmon-polariton waveguide, a plasmon nanolaser based on a plasmonic crystal, and a plasmon sensor of fluorescent biomarkers. lenses, mirrors, detectors, interferometers, waveguides, and lasers. We show that state-of-the-art techniques for the development of plasmon optics elements, which are based on utilizing single-crystal ultrahigh quality metal surfaces, enable us to come closer to the theoretically predicted characteristics of these elements.

Keywords: surface plasmon-polaritons, plasmon optics, elements of plasmon optics

1. Introduction

One extensively developing area of photonics covers the optics of surface plasmon polaritons (SPPs) excited on a metal–dielectric interface [1–3]. The development of surface plasmon wave optics is associated with the creation of its basic elements, which allow controling the properties of plasmon waves, by analogy with photon optics: lenses, mirrors, detectors, interferometers, waveguides, and lasers [4–8]. One of the advantages of plasmon optics lies in its two-dimensionality: plasmon waves propagate on a flat surface, while the transverse localization of a plasmon wave has, as a rule, a subwave scale. This feature has already found important applications for the development of ultrathin photonic elements based on SPPs, such as spectral filters and lenses [7–9]. Another important application of plasmon wave optics is the creation of highly integrated photon circuits [10–12]. The problem of developing highly integrated photonic schemes based on surface plasmon waves involves the creation of various instruments for their generation, control, and processing. The use of plasmon waves is a key factor in this problem, because it combines the field localization on the nanometer scale with a broadband signal transmission [13].

It should be noted that the creation of elements for plasmon optics involves the use of complicated and high-technology equipment: molecular beam epitaxy devices, surface ion etching setups, tightly focused ion beams, electron lithography setups, atomic-force microscopes, high-resolution electron microscopes, and many others. Samples should be studied in high-class (dustless) cleanrooms, because the presence of even single dust particles on the way of SPP propagation can be a source of large losses.

Another important factor in manufacturing elements for plasmon optics concerns the necessity of controling their geometry with nanometer accuracy over distances on the order of the SPP propagation length (about 100 μm in the visible spectral range). These requirements are related to large SPP losses introduced by nano-sized inhomogeneities on a metal surface [14, 15]. This limitation requires the use of single-crystal metal films with atomically smooth surfaces for manufacturing the elements of plasmon optics [16, 17].

P N Melentiev, V I Balykin
Institute of Spectroscopy, Russian Academy of Sciences,
ul. Fizicheskaya 5, 108840 Troitsk, Moscow, Russian Federation;
National Research University "Higher School of Economics"
ul. Myasnitskaya 20, 101000 Moscow, Russian Federation
E-mail: melentiev@isan.troitsk.ru, balykin@isan.troitsk.ru

Received 13 August 2018
Uspekhi Fizicheskikh Nauk **189** (3) 282 – 291 (2019)
DOI: https://doi.org/10.3367/UFNr.2018.06.038415
Translated by M Sapozhnikov; edited by A Radzig

In this paper, we present the main scientific results obtained in recent years by researchers at the Laboratory of Laser Spectroscopy of the Institute of Spectroscopy of the Russian Academy of Sciences in the development and studies of various 2D optical elements for surface plasmon waves. The optical elements were characterized using near and far field methods. It was shown that modern approaches to creating the elements of plasmon optics based on the employment of ultrahigh-quality single-crystal metal surfaces allow us to approach the theoretically predicted parameters of these elements. This, in turn, stimulates the further development of plasmon optics.

2. Optical medium for plasmon waves

Planar plasmon optics is based on the use of plasmon waves propagating along the surface of metallic nanofilms. The surface of a metal film used as an optical medium for surface plasmon waves and its quality are decisive factors for the development of highly integrated SPP-based photonic schemes. The choice of a proper material for preparing a high-quality metal surface is very important. At present, silver and gold are the main materials of experimental nanoplasmonics, because they have minimal ohmic losses among all known natural materials [15].

The preparation of ultrahigh-quality metal nanofilms involves considerable difficulties. Methods for fabricating such films require: (1) an ultrahigh vacuum; (2) special substrates (single-crystal substrates with the crystal lattice period close to that of the material used for preparing a nanofilm); (3) preliminary preparation of the substrate surface (chemical purification, thermal processing in a high vacuum); (4) a certain nanofilm growth rate, and (5) creating conditions for nanofilm relaxation in a high vacuum. If these conditions are not satisfied, optical properties of nanofilms greatly differ from calculated values for an ultrahigh-quality single-crystal metal surface [18].

The development of special technology for growing silver nanofilms [18–21] allowed the preparation of nanofilms with parameters close to predicted theoretical values. The method is based on the epitaxial growth of silver films [19] on the [111] surface of single-crystal silicon, providing the production of high-quality single-crystal silver nanofilms.

The quality of nanofilms created can be characterized by measuring the plasmon-wave propagation length along their surfaces The measurement of the plasmon wave propagation length is a rather complicated problem including the efficient excitation of a plasmon wave in a nanofilm and measurement of the plasmon wave propagation length. One of the most accessible, illustrative, and informative methods consists in the measurement of the propagation length of a plasmon wave excited by laser radiation through an array of nanoslits made in a metal film and detected with the aid of nanogrooves or nanopits located at a certain distance from the slit array [22]. In this method, the interaction of laser radiation with the nanoslit array leads to the excitation of a plasmon wave. The scattering of the plasmon wave by specially made nanogrooves (SPP detectors) and the far-field registering of this scattering allow the SPP propagation length to be measured. This method, in fact, is the optical microscopy of plasmon waves and is used to visualize the propagation of the plasmon wave.

Figure 1 displays the results of measuring the propagation length of a plasmon wave along a silver film surface. The SPP was excited by a cw diode laser with a wavelength of 780 nm

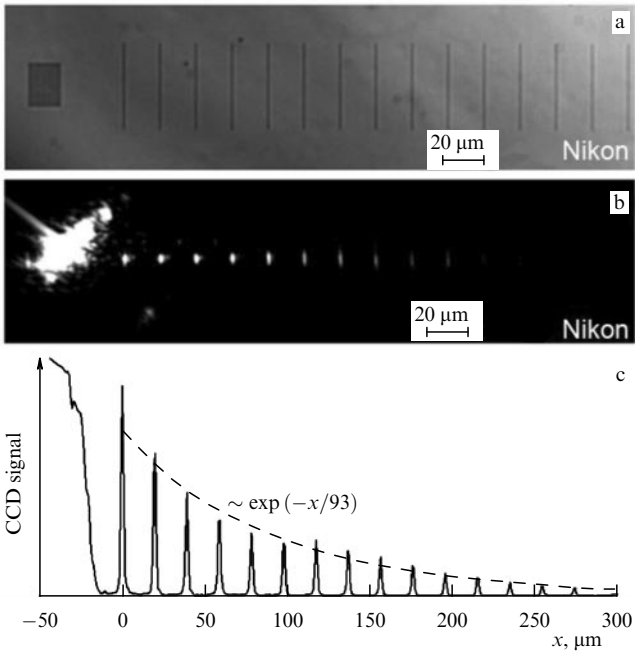

Figure 1. (a) Image of a silver film with nanostructures; (b) image of a silver film upon excitation of a plasmon wave by laser radiation; and (c) cut of the image in Fig. 1b along the plasmon wave propagation; the dashed curve is an exponential approximation with a decay length of 93 μm [18].

focused on an array of nanoslits. The array period was chosen so that the normally incident laser beam excited a plasmon wave on the silver film surface. A series of parallel nanogrooves was made on the propagation path of the plasmon wave. The plasmon wave interacts with nanogrooves and is scattered by them. Radiation scattered by a nanogroove is proportional to the plasmon wave intensity in the nanogroove location, which allows measuring the change in the plasmon wave intensity during its propagation.

Figure 1a demonstrates a silver film with nanostructures made on it: an array with nanoslits for exciting a plasmon wave (seen as a rectangle), and nanogrooves arranged parallel to nanoslits. The scattering of the plasmon wave by nanogrooves makes possible the visualization of a wave and the measurement of its propagation length. Figure 1b shows the silver film surface upon laser excitation of the plasmon wave. The dependence of change in the scattered signal is well approximated by the exponential with the characteristic parameter of 93 μm (the distance at which the signal decreases by a factor of e; see Fig. 1c). The wave propagation length is determined by three factors: the plasmon wave decay caused by losses in the silver film, losses in nanopits, and the diffraction divergence of SPPs. The plasmon wave propagation length determined only by losses in the silver film was calculated from our experiments to be 194 ± 23 μm. This corresponds to calculations [23]. The measurements performed convincingly demonstrate the extremely high quality of silver films prepared by this method [18–21]. This opens up new possibilities in the development of nanoplasmonics based on the employment of low-loss silver films.

3. Plasmon interferometer

Interferometric measurements are inherent in all types of optics (photonic, atomic, etc.), because they permit determin-

ing the basic parameters of waves, such as wavelength, phase velocity, and coherence. The results of these measurements can be used to characterize the properties of a medium in which waves propagate. After the development of the technology of creating single-crystal surfaces of metals in plasmonics, it became possible to conduct interferometric measurements in plasmonics [24, 25]. In this section, we consider interferometric measurements of plasmon waves excited by ultrashort laser pulses of the duration less than 10 fs.

The SPP pulse duration is equal to the exciting laser pulse duration if the response of the electron subsystem changed by 'in metal' is fast. It is known that typical relaxation times of free electrons in a metal can lie in the subfemtosecond range [26], which makes possible excitation of femtosecond plasmon pulses. This requires SPP excitation with the aid of a plasmonic element having the minimal time response. Such elements are nanoslits and nanopits made in a metal film. It is well known that in these elements there are no localized plasmon resonances, and therefore their time response is determined by the relaxation time of free electrons in the metal [3, 8].

The minimal laser pulse duration is known to reach approximately two oscillation cycles of the light wave. A two-cycle laser pulse in the visible region has a broad spectrum in the range from 650 nm to 1 μm and a duration of about 6 fs. Radiation with such parameters has been used to excite plasmon waves and conduct their interferometry on the [111] surface of a single-crystal gold film. Notice the technical difficulties encountered in the use of ultrashort laser pulses in nanoplasmonics, such as the necessity to compensate for the group velocity dispersion of spectral components of a laser pulse and the use of refractive optical elements [27, 28].

Figure 2 schematically depicts a plasmon interferometer formed on a metal film by a through slit and a groove located at an angle to this slit. Such an interferometer operates in the following way [24, 25]. The interferometer is illuminated by laser radiation with the wave vector perpendicular to the film plane. The scattering of laser light by the groove leads to excitation of a surface plasmon wave with the wave vector k_{sp} perpendicular to the groove. The plasmon wave propagating from the groove to the slit is partially scattered from the slit, producing a near-field with amplitude E_2 in the nanoslit region.

Because of the angle α between the slit and groove, the distance traveled by the plasmon wave from the groove to the slit along the x-axis linearly depends on the coordinate x as $d(x) = d_0 + x\sin\alpha$, where d_0 is the minimum distance between the slit and groove. This also leads to the dependence of the field amplitude and phase on the coordinate x in the form $E_2(x) \sim \exp(-k''_{sp}d(x))$ and $\Phi(x) = k'_{sp}d(x) + \phi_0$, respectively. The presence of the angle between the slit and groove results in interference of near-fields from laser radiation in the slit and the surface plasmon wave propagating from the groove. The dependence of the interference pattern intensity on the coordinate takes the form

$$I(x) = E_1^2(x) + E_2^2(x) + 2E_1(x)\,E_2(x)\,\cos(\Phi(x))\,, \qquad (1)$$

where $E_1(x)$ is the near-field amplitude of laser radiation in the slit. The interference term in formula (1) has a spatial period described by the expression

$$T_x = \frac{2\pi}{k'_{sp}\sin\alpha}\,. \qquad (2)$$

Figure 3a displays an electron-microscope image of a plasmon interferometer [25], and Fig. 3b presents an interference pattern obtained by illuminating the interferometer by a cw laser. Figure 3b shows that the optical image contains a rather large number of interference maxima and minima. When cw laser radiation is used, this number is determined by the plasmon-wave propagation length along the gold film surface and by the SPP wave vector [25]. For laser pulse durations of less than 50 fs, the number of interference minima and maxima becomes proportional to the pulse duration. This allows using a plasmon interferometer to measure the duration of ultrashort laser pulses. The possibility of measuring the duration of ultrashort 6-fs laser pulses consisting of only two light wave cycles has also been demonstrated [25].

The measurement of the laser pulse durations with the aid of plasmon interferometry also forms the basis for the method of controling laser radiation parameters in nanoplasmonic experiments. In such experiments, it is important to measure the pulse duration directly in the plane of a sample under study (as a rule, in the focal plane of a microscope), which advantageously distinguishes this method from other known methods for measuring laser pulse durations [29–31].

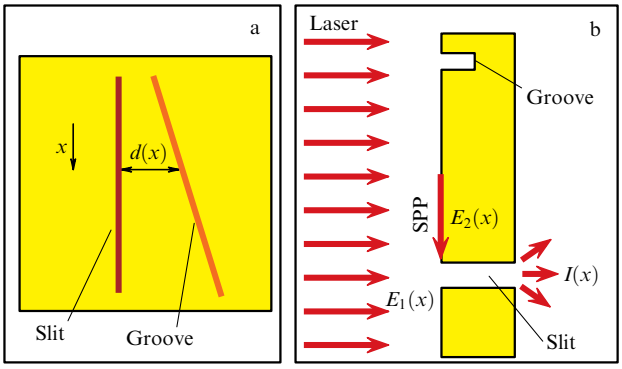

Figure 2. Schematic of a plasmon interferometer: (a) top view, (b) excitation scheme [25].

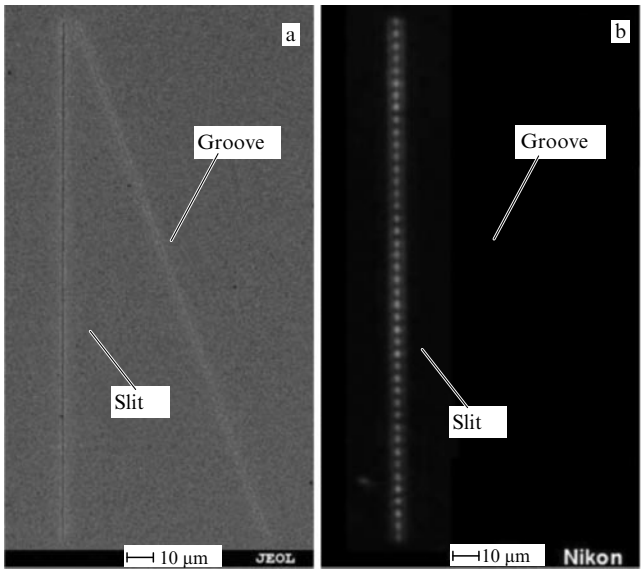

Figure 3. (a) Electron image of a plasmon interferometer; (b) interference pattern upon illumination of the interferometer with a laser beam [25].

4. Focusing of surface plasmon waves onto a diffraction-limited spot

The focusing of waves is one of the most important tasks in optics of any type (photon, atomic, charged particle), and in plasmon optics it allows one to couple a propagating plane wave with a spatially localized wave. In plasmon optics, focusing is implemented by surface structuring of a metal film in the form of a bent comb, bent slit, or bent chain of nanoparticles, with the help of a dielectric lens created on the metal surface, similarly to photonic optics, or by involving several focusing elements [32–36]. An important optical element for wave focusing is a parabolic mirror. Parabolic mirrors are widely employed in photon optics and, unlike other focusing elements, provide wave focusing onto a diffraction-limited spot and have no chromatic or spherical aberrations. In nanoplasmonics, parabolic mirrors have not been realized so far. We demonstrated the efficient control of plasmon waves using a parabolic mirror. Such a mirror provides SPP reflection with an efficiency up to 30%, SPP focusing onto a diffraction-limited spot about the wavelength λ_{SPP} in size, and spatial scanning of the SPP focal region [32].

Plasmon wave focusing with the aid of a parabolic plasmon mirror is sketched in Fig. 4a, where the electron-microscope image of an experimental sample is shown. The sample represents a 200-nm thick silver film with the following elements created on its surface: an array of nanoholes for excitation of plasmon waves; a parabolic mirror-nanogroove (100 nm in width and 120 nm in depth) with a focal distance of 20 μm; five detectors-nanogrooves located in the region of assumed plasmon wave focusing (60 nm in width and 25 nm in depth), and a nanocavern (60 nm in diameter and 25 nm in depth) for identifying the plasmon wave propagation on the nanofilm surface.

Figure 4b shows the results of measuring plasmon wave focusing with the help of a parabolic mirror. The optical image was obtained by illuminating a sample by 800-nm laser radiation polarized along the lines of the array with nanoholes. The laser spot diameter corresponds to the size of the nanohole array and equals 20 μm. The bright spot in the figure corresponds to light transmission through the nanohole array. To the left of this spot are located points of the same size arranged in the array order. These points correspond to a plasmon wave propagating over the silver film surface and scattered by nanopits; they indicate the propagation of the plasmon wave on the film surface. The figure also displays the signal of plasmon wave scattering from a mirror-nanogroove. Bright spots in the location of detectors-nanogrooves correspond to the scattering of the focused plasmon wave. The bright spots allow one to determine the size and position of the plasmon wave waist in the focus.

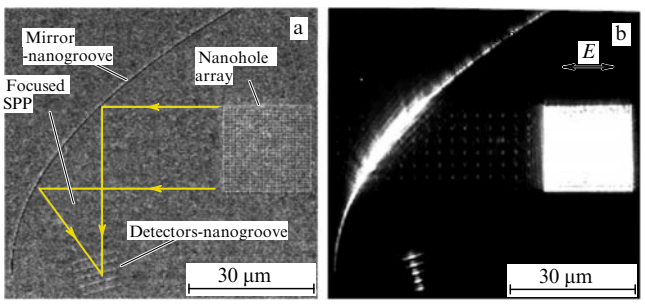

Figure 4. SPP focusing with a plasmon mirror. (a) Electron image of an experimental sample; (b) optical image of an experimental sample excited by an 800-nm laser radiation [32].

We have demonstrated SPP focusing with several parabolic mirrors having focal distances of 20, 10, and 5 μm. A plasmon mirror with a focal distance of 20 μm allows focusing a plasmon wave into a spot 1.2 μm in size. A decrease in the focal distance of the plasmon mirror to 10 μm results in a decrease in the focal spot to 400 nm. This value is half the plasmon wavelength, i.e., the plasmon mirror with the focal distance of 10 μm allows us to focus the plasmon wave into a spot with a diffraction-limited size. Further reduction of the focal length of a parabolic mirror leads to deterioration of focusing, which is associated with the manifestation of boundary effects caused by the closeness of the plasmon mirror edge to the plasmon wave focusing region.

An important property of plasmon wave focusing with the help of a parabolic mirror consists in the possibility of controling the position of the focusing region. It was shown in Ref. [32] that small deviations of a laser beam exciting a plasmon wave by the angle θ from the normal cause a corresponding change in the plasmon wave propagation direction by the angle $\alpha \approx (\Lambda/\lambda)\,\theta$, where Λ is the period of location of nanoholes in the array used for SPP excitation by laser radiation. As a result, the position of the plasmon wave focusing spot is displaced. It was possible to displace the plasmon wave focusing spot by distances of up to 5 μm. This approach to plasmon wave control opens up new possibilities for developing complex optical setups using SPPs in all-optical devices and elements.

5. Plasmon waveguides

The optics of surface plasmon waves represents an extensively developing field of integrated optics [4–8]. The key element of integrated plasmonics is a plasmon waveguide. The specific features of plasmon waveguides are subwavelength field localization in the waveguide cross section and considerable ohmic losses in metal parts of the waveguide restricting the wave propagation length. As a rule, an increase in the field localization degree in the cross section of a plasmon waveguide results in a decrease in the wave propagation length in the waveguide [37]. As the transverse localization of the mode increases, the wave field penetrates more deeply into metal parts of the waveguide, resulting in an increase in the ohmic losses of the wave.

A dielectrically loaded surface plasmon–polariton waveguide (DLSPPW) is a promising type of plasmon waveguide providing a considerable propagation length of a plasmon wave along with its subwavelength transverse localization [37]. A DLSPPW is a dielectric ridge mounted on a flat metal surface (Fig. 5a). Figure 5b displays the electric field distribution for the fundamental mode of the DLSPPW in its cross section [38].

Theoretical estimates have revealed that the values of the width $w = 110$ nm and height $h = 120$ nm are optimal for a DLSPPW, because they provide good spatial localization of the mode along with a large propagation length of the wave. For these values of w and h, the main parameters of the plasmon mode become the propagation length $L_{mode} = 81.9$ μm and the mode size $w_{mode} = 670$ nm. A DLSPPW with such geometrical parameters is a spatially single-mode plasmon waveguide. The mode field distribution of such a waveguide is presented in Fig. 5b.

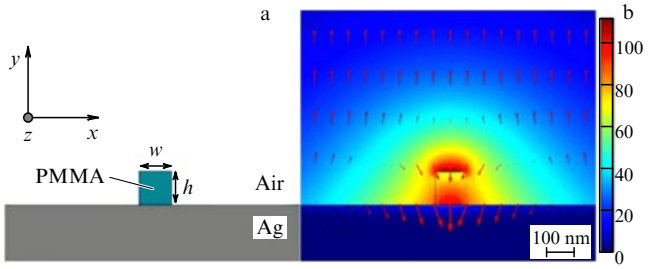

Figure 5. (a) Transverse cut of the DLSPPW. The dielectric ridge of width w and height h is located on a silver film no less than 200 nm in thickness; (b) electrical field amplitude distribution for the fundamental mode in the cross section of the DLSPPW with $h = 120$ nm and $w = 110$ nm at $\lambda = 78$ nm. The arrows mark the direction of the electric field projected onto the xy plane [38]. PMMA: polymethyl methacrylate.

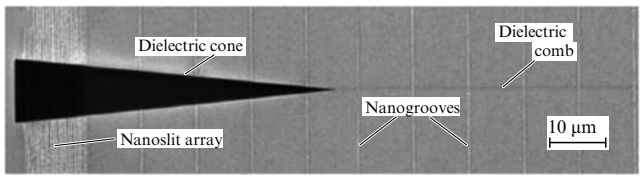

Figure 6. Electron image of an experimental sample with the DLSPPW: array of nanoslits, nanogrooves, dielectric cone, and DLSPPW [38].

Experimental DLSPPW samples were prepared in a few stages (Fig. 6). First, a 200-nm silver film was deposited. Two types of silver films were used: a single-crystal film deposited onto a mica substrate, and a polycrystalline film deposited onto an atomically smooth sapphire substrate. Measurements with a plasmon interferometer [25] have shown that a polycrystalline silver film on an atomically smooth sapphire substrate features better optical properties, and for this reason this film was utilized to manufacture plasmon waveguides.

At the second stage of sample manufacturing, an array of nanoslits and a set of nanogrooves were produced in the direction perpendicular to the waveguide axis. Then, at the third stage, the silver film was covered with a 120-nm polymethyl methacrylate (PMMA) layer in which the dielectric parts of the structure (the taper and DLSPPW) were manufactured by the method of electron-beam lithography.

Figure 6 shows an electron image of one of the structures with a plasmon waveguide. The figure demonstrates the array of nanoslits, nanogrooves, dielectric taper, and DLSPPW. The distance between the nanoslits was 10 μm. Nanogrooves were made to visualize the plasmon wave propagation in the DLSPPW and measure its propagation length (plasmon wave microscopy with the aid of nanostructures). The plasmon wave in the DLSPPW is scattered by nanogrooves and scattered radiation is detected in the far-field. Thus, nanogrooves serve as the local probes of the plasmon wave field. The plasmon wave propagation length in the DLSPPW was determined from the z-coordinate dependence of the intensity of the plasmon field scattered by nanoslits. The nanoarray in the cone served for exciting a plasmon wave with a laser beam. The number of nanoslits in the array was $N_{\text{slits}} = 20$. The width of the taper base was 11.3 μm, and the taper length was $l_{\text{tap}} = 60$ μm. For an array with a period of 550 nm and slit width $a = 150$ nm, the plasmon wave excitation efficiency has its maximum at $\lambda = 780$ nm. A plasmon wave excited by laser radiation is focused onto the DCLSOOW.

Figure 7 presents the results of measuring excitation and propagation parameters of a plasmon wave in the DLSPPW. Optical images in Figs 7a, b were obtained for different exposure times of a CCD camera used for waveguide visualization. The geometry of the structure was visualized with a white light source. Figures 7a, b demonstrate the plasmon wave scattering by nanoslits. Figure 7c illustrates the propagation and decay of the plasmon wave in the DLSPPW: the dependence of the intensity of the plasmon wave scattering on the z-ordinate is shown. Bright 'peaks' observed in Fig. 7c appear due to plasmon wave scattering by nanoslits. The consideration of plasmon wave losses due to its scattering by nanoslits (about 5% of the wave power for each nanoslit) allows one to determine the wave propagation length in the waveguide, which amounts to $L_{\text{SPP}} \approx 30$ μm.

Compared to other configurations of the guided propagation of plasmon waves, the configuration presented here offers two substantial advantages. First, there is the possibi-

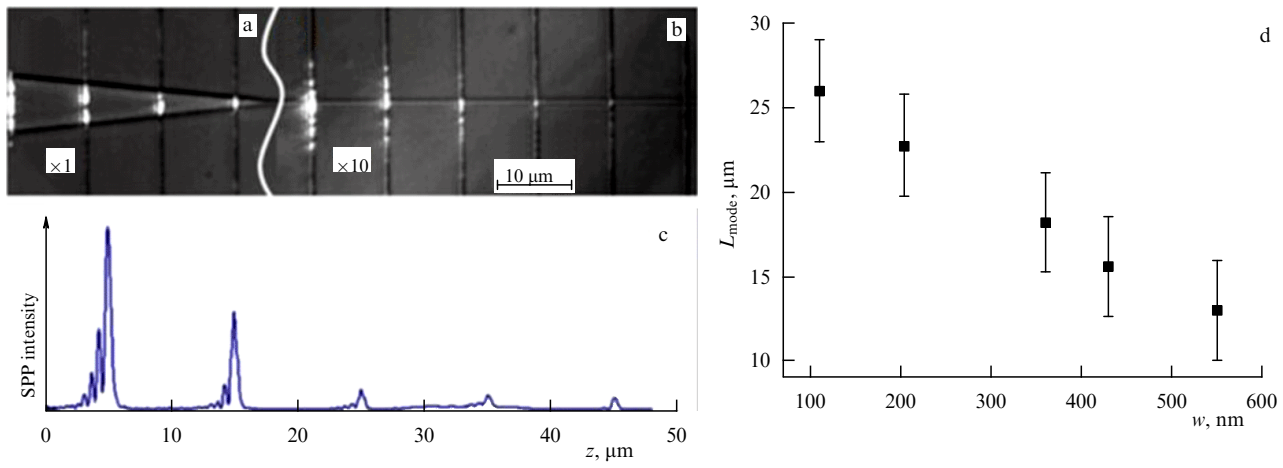

Figure 7. Results of measuring the parameters of the excitation and propagation of a plasmon wave in the DLSPPW: (a) optical image showing the plasmon wave propagation in a taper, and (b) the DLSPPW; (c) intensities of scattering of a plasmon wave by nanogrooves showing the wave propagation and decay in the waveguide; (d) dependence of the propagation length of the plasmon mode in the DLSPPW on the dielectric ridge width [38].

lity of using an optically thick metal film, which excludes losses related to plasmon wave leakage into the substrate. Second, this configuration takes advantage of laser excitation of the waveguide from the substrate side, which considerably reduces the parasitic illumination of the waveguide by the scattered radiation [22].

6. Plasmon crystal nanolaser

A huge amount of research over the last two decades has been devoted to the development of new extremely small lasers. The greatest progress has been achieved in the field of semiconductor lasers [39–42]. A fundamentally new approach to the miniaturization of lasers is based on applying plasmon fields instead of photon fields.

A plasmon nanolaser is a nanoscale (at least in one dimension) quantum generator of coherent plasmon fields. A plasmon nanolaser nanoscopic in all three dimensions is also called a spaser (Surface Plasmon Amplification by Stimulated Emission of Radiation) [43]. The idea of a plasmon nanolaser was first proposed by Sudarkin and Demkovich [44]. The possibility of creating a spaser was theoretically substantiated by Stockman and Bergman [43]. The operation of a spaser was demonstrated for the first time by Noginov and co-authors [45]. To date, plasmon nanolasers have been demonstrated in numerous experiments. A number of reviews devoted to plasmon nanolasers have already been published [42, 46–53].

A 3D nanolaser can be extremely small, consisting only of a few hundred atoms. In this case, the generated energy, both its near-field part and the laser emission energy, is extremely small. We can assume that, using a regular structure consisting of individual nanoparticles (spasers), it is possible simultaneously to increase the output power and control the directivity of emission of an ensemble of spasers. Plasmon particles/resonators in the form of a two-dimensional array were considered [54] as a device for generating directional emission. Directional emission of such an array of nanoparticles appears due to in-phase oscillations of individual nanoparticles.

A regular structure consisting of an array of nanoparticles, a plasmon crystal, can be of two types: an array of individual metal nanoparticles or a complementary Babine structure created in a metal film — an array of nanoholes. It is known that the thermal destruction of a metal nanostructure occurs at lower radiation intensities than in a Babine complementary structure created in a metal film [14, 55]. Thus, upon laser illumination of a nanorod, its temperature proves to be a few orders of magnitude higher than in a complementary structure in the form of a nanoslit [55]. Therefore, a plasmon crystal based on a structured nanofilm is more preferable for building a nanolaser than an array of nanoparticles.

Lasing in plasmon crystals based on an array of metal holes is demonstrated experimentally in Refs [56–59]. A diagram of such a plasmon nanolaser is shown in Fig. 8 [56]. An experimental nanolaser sample was manufactured in several stages. An indium–gallium arsenide (InGaAs) layer was deposited onto an indium phosphide (InP) plate and was then covered with a thin InP layer. After that, a silicon nitride (SiN) protective layer was deposited. The protective layer was covered with a gold film in which an array of nanoholes was formed. The indium–gallium arsenide layer served as an active medium of the nanolaser pumped at 1.06 μm. The

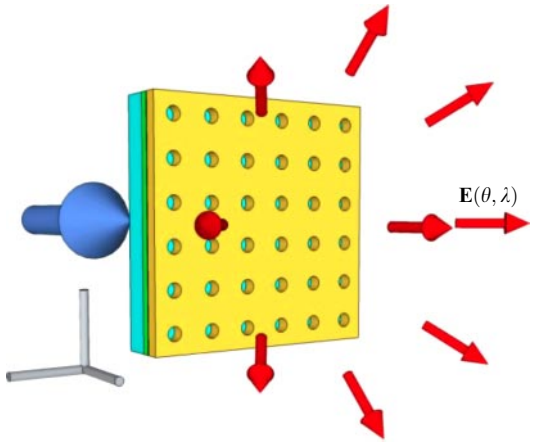

Figure 8. Plasmon crystal nanolaser formed by an array of nanoholes in a metal film [56].

lasing threshold was determined from the dependence of the lasing power on the pump power.

Dye molecules are the best quantum emitters for the active medium in nanolasers, because they can have a quantum efficiency of about 100% and can be used to create optically homogeneous media with high molecular densities. A considerable disadvantage of dye molecules as active media is their photoinduced bleaching, when the dye molecules cease to absorb radiation (after $10^5 - 10^6$ photon absorption–emission events) [60].

We have demonstrated a planar plasmon nanolaser based on a plasmon crystal made of an array of nanoholes with a solution of dye molecules as the active medium. The active medium in the liquid state offers a number of fundamental advantages over solid active media. First, the active medium in the form of a solution of dye molecules weakens the dye bleaching effect by many orders of magnitude, providing the creation of a stable active medium, as opposed to a solid matrix doped with dye molecules. Second, it is possible to introduce an analyte to the solution, realizing the concept of intracavity plasmon spectroscopy [58].

Figure 9a illustrates a plasmon crystal nanolaser with an active medium in the form of a solution of dye molecules. The plasmon crystal is formed by an array of 150-nm nanoholes made in a silver film on a dielectric substrate. The period of the nanohole array is $\Lambda = 565$ nm. The active medium was a solution of R101 dye molecules in a DMSO (dimethyl sulfoxide) solvent producing amplification up to 75 cm^{-1} upon pumping by 530-nm, 10-ns laser pulses with a pulse repetition rate of 40 Hz. The volume of the dye solution excitation region is four orders of magnitude smaller than the total volume of the active medium. Such a volume ratio provides the long-time stable generation of the nanolaser up to several weeks due to diffusion of dye molecules.

Figure 10b presents the emission spectra of the nanolaser for two pump intensities: 60 kW cm^{-2} (red curve (*1*)), luminescence signal magnified by a factor of 100) and 2.5 MW cm^{-2} (blue curve (*2*)). One can see that for low pump intensities (below 150 kW cm^{-2}) the spectral profile of a luminescence line coincides with that of the R101 dye. For higher pump intensities, the shape of the luminescence spectrum strongly changes and a narrow line appears at 628 nm. In addition, the nanolaser exhibits a threshold dependence of its emission on the pump intensity and also

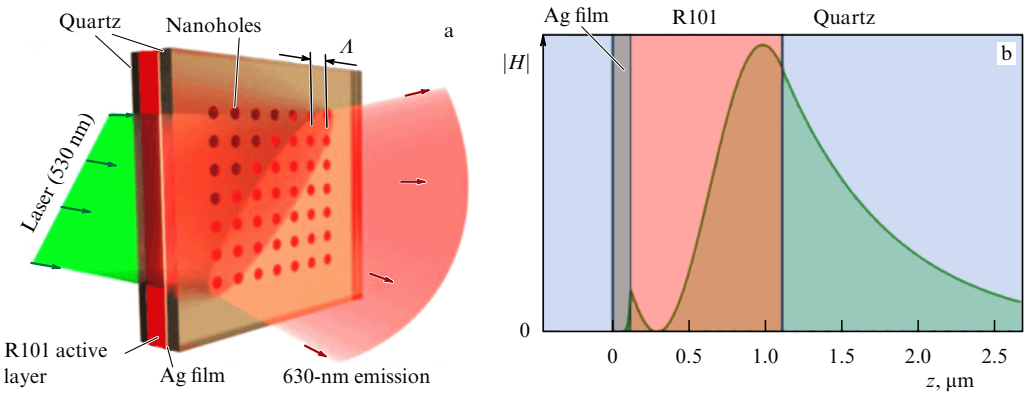

Figure 9. (a) Plasmon nanolaser formed by an array of nanoholes in a silver film; (b) spatial distribution of the field H for the TM mode in the 'silver film–active medium–quartz substrate' system [58].

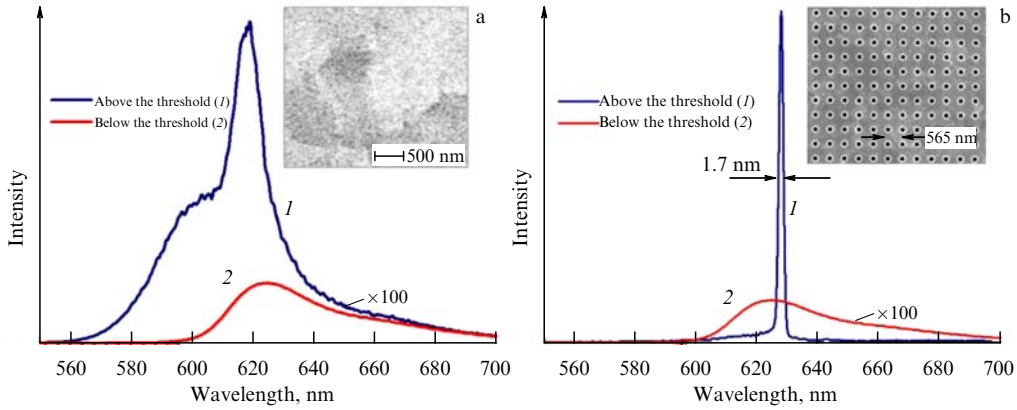

Figure 10. (Color online.) Emission dynamics of a plasmon nanolaser: (a) luminescence spectrum of dye molecules in the hybrid mode of experimental plasmon nanolaser sample without nanoholes; (b) luminescence spectrum of a plasmon nanolaser. Insets show electron images of the surface of samples under study [58].

high emission directivity (about 1.3°) upon pumping above the threshold, which is inherent in lasing [58].

Thus, we have shown that, using a high-Q plasmon crystal, the optimized excitation scheme, and an R101 dye solution as the active medium, we created a plasmon nanolaser with extremely low mode losses (about 40 cm^{-1}), emitting in one of the most 'inconvenient' spectral regions in nanoplasmonics ($\sim$ 630 nm), characterized by high losses in metals.

7. Plasmon sensor of biomolecules based on a plasmon nanolaser

The dynamics of a plasmon laser is similar in many respects to that of conventional lasers [43, 45, 61–64]. Similarly to conventional lasers, a sensorics based on plasmon lasers was proposed and theoretically studied in Refs [65–67]. It was shown that the use of plasmon nanolasers for intracavity laser spectroscopy provides an increase in the plasmon sensor efficiency by two orders of magnitude.

The application of a plasmon nanolaser for the intracavity sensorics was first demonstrated in paper [58], where a plasmon laser played the part of a sensor chip in which an analyte under study was added to a cavity with a liquid active medium. The nanolaser resonator was an array of nanoholes in a silver film (Fig. 9). In such a sensor, pumping of the active medium solution with an analyte is realized, which ensures both maximum sensitivity and repeated use of such a sensor. The subwavelength scale of the plasmon mode of the nanolaser and microfluidics technology are attractive and promising for constructing the 'chip-based laboratory' [68, 69].

Schematic of the sensor is presented in the inset to Fig. 11. The active medium was a solution of R101 dye molecules in DMSO at a concentration of 800 ppm. The plasmon nanolaser was pumped by 532-nm laser pulses (Fig. 9). When the pump intensity exceeded the threshold, lasing at a wavelength of 628 nm appeared. Cy-5 dye with a broad absorption band near the lasing frequency was utilized as an analyte. The addition of the analyte leads to additional losses in the plasmon laser resonator and changes the lasing regime. The analyte volume added to the sensor was less than 1 μl.

Figure 11 illustrates the emission dynamics of a plasmon nanolaser at three analyte concentrations: 7 and 0.7 ppm, and 70 ppb. It can be seen that the analyte addition reduces the plasmon laser intensity. The minimal concentration of 70 ppb detected with this sensor demonstrates the ultrahigh analyte detection sensitivity.

The Cy-5 dye molecules employed in this plasmon sensor are known as fluorescent biomarkers [70]. Such molecules can be attached via corresponding antibodies to various biomolecules, which then serve as markers of different processes in the human body [71]. Thus, this plasmon sensor can be used for medical applications with a small blood plasma volumes and analyses performed with the highest sensitivity.

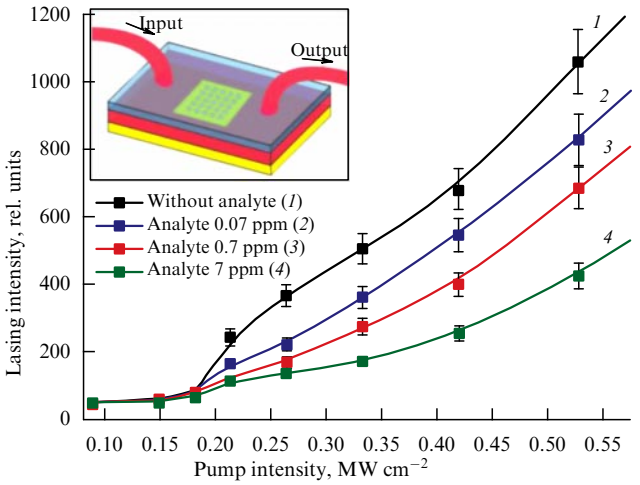

Figure 11. Dependences of the plasmon nanolaser intensity on pump intensity at different Cy-5 dye concentrations in a nanolaser resonator. The inset shows a diagram of an analyte addition to the plasmon nanolaser resonator [58].

8. Conclusion

We have presented the results of studies performed in recent years at the Laboratory of Laser Spectroscopy of the Institute of Spectroscopy, RAS on the development and investigation of optical elements for surface plasmon waves, an optical medium for plasmon waves, a plasmon interferometer, a parabolic plasmon mirror for focusing plasmon waves, a dielectrically loaded plasmon–polariton waveguide, a plasmon crystal nanolaser, and a plasmon sensor for fluorescent biomarkers. Relevant work is being continued in our Laboratory at present. It is expected that significant scientific and applied results will be obtained in the field of quantum nanoplasmonics [72] and plasmon biosensorics with a sensitivity at the level of single molecules [73, 74]. Today, the high-speed performance with a large spatial localization of the elements of nanoplasmonics is not achievable by other approaches, so the plasmon nanooptics will actively develop despite of the great technological difficulties.

Acknowledgments

The authors are deeply grateful to the researchers at the Laboratory of Laser Spectroscopy: A E Afanas'ev, A S Kalmykov, A S Gritchenko, L V Son, and D V Kudryavtsev, who are engaged in studies presented in this paper.

References

1. Agranovich V M, Mills D L *Surface Polaritons. Electromagnetic Waves at Surface and Interfaces* (Amsterdam: North-Holland, 1982)
2. Ditlbacher H et al. *Appl. Phys. Lett.* **81** 1762 (2002)
3. Klimov V *Nanoplasmonics* (New York: Pan Stanford, 2014)
4. Krenn J R et al. *J. Microscopy* **209** 167 (2003)
5. Barnes W L, Dereux A, Ebbesen T W *Nature* **424** 824 (2003)
6. Zayats A V, Smolyaninov I I, Maradudin A A *Phys. Rep.* **408** 131 (2005)
7. Lal S, Link S, Halas N J *Nature Photon.* **1** 641 (2007)
8. Maier S A *Plasmonics. Fundamentals and Applications* (Berlin: Springer, 2007)
9. Stockman M I *Phys. Today* **64** (2) 39 (2011)
10. Zia R et al. *Mater. Today* **9** (7–8) 20 (2006)
11. Atwater H A *Sci. Am.* **296** (4) 56 (2007)
12. Brongersma M L, Shalaev V M *Science* **328** 440 (2010)
13. Gramotnev D K, Bozhevolnyi S I *Nature Photon.* **4** 83 (2010)
14. Melentiev P N et al. *Opt. Express* **21** 13896 (2013)
15. Balykin V I, Melentiev P N *Phys. Usp.* **61** 133 (2018); *Usp. Fiz. Nauk* **188** 143 (2018)
16. Vesseur E J R et al. *Appl. Phys. Lett.* **92** 083110 (2008)
17. Huang J-S et al. *Nature Commun.* **1** 150 (2010)
18. Baburin A S et al. *Opt. Mater. Express* **8** 3254 (2018)
19. Rodionov I A et al. *Int. Soc. Opt. Photon.* **10343** 1034337 (2017)
20. Baburin A S et al., in *Progress In Electromagnetics Research Symp.–Spring, PIERS, 2017* (Piscataway, NJ: IEEE, 2017) p. 1497
21. Rodionov I A et al., arXiv:1806.07611
22. Melentiev P N, Kuzin A A, Balykin V I *Quantum Electron.* **47** 266 (2017); *Kvantovaya Elektron.* **47** 266 (2017)
23. Babar S, Weaver J H *Appl. Opt.* **54** 477 (2015)
24. Temnov V V et al. *Opt. Express* **17** 8423 (2009)
25. Melentiev P N et al. *Opt. Commun.* **382** 509 (2017)
26. Stockman M I et al. *Nature Photon.* **1** 539 (2007)
27. Melentiev P N et al. *Nano Lett.* **16** 1138 (2016)
28. Melentiev P N et al. *Laser Phys. Lett.* **11** 105301 (2014)
29. Bowlan P, Gabolde P, Trebino R *Opt. Express* **15** 10219 (2007)
30. Extermann J et al. *Opt. Express* **16** 10405 (2008)
31. Li H et al. *Appl. Phys. Lett.* **96** 021103 (2010)
32. Melentiev P N, Kuzin A A, Negrov D V, Balykin V I *Plasmonics* **13** 2361 (2018)
33. Radko I P et al. *Opt. Express* **17** 7228 (2009)
34. Evlyukhin A B et al. *Opt. Express* **15** 16667 (2007)
35. Kim H, Hahn J, Lee B *Opt. Express* **16** 3049 (2008)
36. Lewandowski W et al. *Nature Commun.* **6** 6590 (2015)
37. Holmgaard T, Bozhevolnyi S I *Phys. Rev. B* **75** 245405 (2007)
38. Melentiev P N et al. *Laser Phys. Lett.* **14** 126201 (2017)
39. Strauf S, Jahnke F *Laser Photon. Rev.* **5** 607 (2011)
40. Khajavikhan M et al. *Nature* **482** 204 (2012)
41. Schneider C et al. *Nature* **497** 348 (2013)
42. Balykin V I *Phys. Usp.* **61** 846 (2018); *Usp. Fiz. Nauk* **188** 935 (2018)
43. Bergman D J, Stockman M I *Phys. Rev. Lett.* **90** 027402 (2003)
44. Sudarkin A N, Demkovich P A *Sov. Phys. Tech. Phys.* **34** 764 (1989); *Zh. Tekh. Fiz.* **59** (7) 86 (1989)
45. Noginov M A et al. *Nature* **460** 1110 (2009)
46. Oulton R F *Mater. Today* **15** (1–2) 26 (2012)
47. Vinogradov A P et al. *Phys. Usp.* **55** 1046 (2012); *Usp. Fiz. Nauk* **182** 1122 (2012)
48. Protsenko I E *Phys. Usp.* **55** 1040 (2012); *Usp. Fiz. Nauk* **182** 1116 (2012)
49. Ma R-M et al. *Laser Photon. Rev.* **7** 1 (2013)
50. Berini P, De Leon I *Nature Photon.* **6** 16 (2012)
51. Tame M S et al. *Nature Phys.* **9** 329 (2013)
52. Gwo S, Shih C-K *Rep. Prog. Phys.* **79** 086501 (2016)
53. Premaratne M, Stockman M I *Adv. Opt. Photon.* **9** 79 (2017)
54. Zheludev N I et al. *Nature Photon.* **2** 351 (2008)
55. Melentiev P N et al. *Laser Phys. Lett.* **10** 075901 (2013)
56. van Beijnum F et al. *Phys. Rev. Lett.* **110** 206802 (2013)
57. Meng X et al. *Laser Photon. Rev.* **8** 896 (2014)
58. Melentiev P et al. *Appl. Phys. Lett.* **111** 213104 (2017)
59. Baburin A S et al. *Proc. SPIE* **10672** 106724D (2018)
60. Zondervan R et al. *J. Phys. Chem. A* **108** 1657 (2004)
61. Stockman M I *Nature Photon.* **2** 327 (2008)
62. Stockman M I *Phys. Rev. Lett.* **106** 156802 (2011)
63. Lisyansky A A et al. *Phys. Rev. B* **84** 153409 (2011)
64. Andrianov E S et al. *Phys. Rev. B* **85** 035405 (2012)
65. Lozovik Y E, Nechepurenko I A, Dorofeenko A V *Photon. Nanostruct. Fundam. Appl.* **21** 60 (2016)
66. Lozovik Yu E et al. *Laser Phys. Lett.* **11** 125701 (2014)
67. Lozovik Yu E et al. *Phys. Lett. A* **378** 723 (2014)
68. Srinivasan V, Pamula V K, Fair R B *Lab Chip* **4** 310 (2004)
69. Fair R B *Microfluid. Nanofluid.* **3** 245 (2007)
70. Liu Y et al. *Nanotechnology* **15** 1368 (2004)
71. Sandoval Y et al. *Clin. Chem.* **63** 369 (2017)
72. Bozhevolnyi S I, Khurgin J B *Nature Photon.* **11** 398 (2017)
73. Walt D R *Anal. Chem.* **85** 1258 (2013)
74. Taylor A B, Zijlstra P *ACS Sens.* **2** 1103 (2017)